Int. J. Electrochem. Sci., 14 **(2019)** 6658 – 6666, doi: 10.20964/2019.07.24

International Journal of ELECTROCHEMICAL SCIENCE
www.electrochemsci.org

Two Phase-Diagrams of the Thermal Roughening Transition in Anodic Dissolution of Polycrystalline Nickel

M. Saitou

Department of Mechanical Systems Engineering, University of the Ryukyus
1 Senbaru, Nishihara, Okinawa, 903-0213, Japan
E-mail: saitou@tec.u-ryukyu.ac.jp

Received: 22 February 2019 / *Accepted:* 19 April 2019 / *Published:* 10 June 2019

Two phase-diagrams of the thermal roughening transition on polycrystalline nickel surfaces dissolved anodically under sulfuric acid solution concentrations and temperatures were prepared using a confocal laser scanning microscope (CLSM) and dissolution mass measurement (DMM). One phase diagram shows the transition between polycrystalline surfaces free of grooves formed by preferential grain boundary dissolution and those with grain boundary grooves. Solution concentrations and temperatures at which no formation of grain boundary grooves occurred were demonstrated. The other phase diagram shows stable states among smooth surfaces, rough surfaces, and combined smooth and rough surfaces. CLSM and DMM analyses demonstrated that the transition from smooth surfaces to rough surfaces caused a drastic change in dissolution mass and was attributed to a change in dissolution modes from the motion of kink-antikink pairs to the random formation of adatom-vacancy pairs.

Keywords: Thermal roughening transition; Phase diagram; Grain boundary grooves; Kink-antikink pair; Adatom-vacancy pair

1. INTRODUCTION

Nickel and nickel oxide surfaces formed by a variety of methods have attracted research attention owing to their potential applications in lotus effect materials [1], antibacterial materials [2], p-type semiconductors [3], catalytic materials [4], and porous materials [5]. Among the various methods for the formation of the nickel and nickel oxide surfaces, anodic dissolution has often been carried out.

In the anodic dissolution of polycrystalline nickel, the dissolution initially starts at grain boundaries and then forms grain boundary grooves [6–7]. This is because the grain boundary energy is larger than the surface energy [8–9] and polycrystalline nickel starts dissolving at a smaller applied potential. After the anodic dissolution of polycrystalline nickel, grain boundary grooves are observed as lines using a light microscope. The dissolution of polycrystalline nickel in sulfuric acid solution occurs

with the activation energy [10]. This study investigates whether etched polycrystalline surfaces with no grooves can be obtained in anodic dissolution under chosen temperatures and sulfuric acid solution concentrations.

It has been reported that for nickel surfaces formed by the anodic dissolution, the surface roughness obeys a scaling law characterized by exponents that represent a universal class [11–12]. The surface roughening transition from a smooth to the rough surface occurs at a transition temperature. For example, in an ideal surface, a kink and adatom pair (KAP) and adatom-vacancy pair (AVP) are spontaneously formed [13] through a basic thermal excitation known as the Kosterlitz-Thouless (KT) transition [14]. In fact, in a smooth surface at an atomic level, one of the basic excitations has been found to be the formation of AVP [15–16]. The formation of KAP and AVP markedly influences the surface states.

We reported the thermal roughening transition of nickel surfaces dissolved anodically in sulfuric acid solution using a rectangular pulse current [17]. However, phase diagrams that represent surface states formed by KAP and AVP under different temperatures and sulfuric acid solution concentrations have not been studied.

In the anodic dissolution of nickel in sulfuric acid solution, the anode is observed to lose weight according to the following electrochemical reaction; $Ni + OH^- \rightarrow Ni^{2+} + OH^- + 2e^-$ [18]. As the two dissolution mechanisms such as the formation of KAP and AVP affect the dissolution rate, the measurement of the dissolution mass leads to a distinct change in the anodic dissolution mass at the transition temperature [17].

The purpose of the present study is to demonstrate two phase diagrams in polycrystalline nickel anodic dissolution: One phase diagram that represents a transition between polycrystalline surfaces free of grain boundary grooves and those with grooves; the other phase diagram that shows stable states among smooth surfaces, rough surfaces, and smooth and rough surfaces under temperatures and sulfuric acid solution concentrations.

2. EXPERIMENTAL SETUP

The experimental procedure was as follows: 30 × 5 and 80 × 50 mm^2 polycrystalline nickel plates (purity 99.95 %) were prepared as the anode and cathode, respectively. The typical root-mean-square (RMS) roughness of the polycrystalline nickel plate before the anodic dissolution was 0.21±0.03 μm and its surface had a mirror-like appearance. The two electrodes were located parallel in an electrochemical cell containing 0.5, 1.0, and 1.7 (mol/L) sulfuric acid solution. Only one side of the anode dissolved because the other side of the anode was coated with an insulating organic thin film to prevent dissolution. The cathode was completely immersed in the sulfuric acid solution. The area of the cathode was about 53 times larger than that of the anode. Hence, the resistance of the electric double layer in series of the cathode in the sulfuric acid solution was ignored in comparison to that in series of the anode. The cell was maintained within a temperature range of 277 – 345 K. Direct current within a current density range of 140 – 300 mA/cm^2 was supplied using a bipolar power source.

After anodic dissolution, dissolution mass measurement (DMM) was performed as follows: The nickel anode was weighed to a precision of 0.1 mg using an electric balance. For example, the mass of nickel dissolved anodically in the sulfuric acid for 234.85 s at a current density of 140 mA/cm^2 becomes 10 mg/cm^2 when the current efficiency is 100 %. Here, the current efficiency is defined as the ratio of the actual amount of nickel dissolved into the solution to that expected from Faraday's law. We called this ratio the normalized dissolution mass, which was determined for a variety of current densities and temperatures. The dissolution mass of 10 mg/cm^2 is equivalent to a dissolution film thickness of 11.2 μm/cm^2.

The surface of dissolved polycrystalline nickel was observed and measured using the confocal laser scanning microscope (CLSM) that was capable of measurements with an accuracy of 0.01 μm in depth. A digitized microscopic image of the nickel surface dissolved anodically was obtained with a resolution of 1024 × 746 pixels.

3. RESULTS AND DISCUSSION

3.1 No grain boundary grooves or groove formation

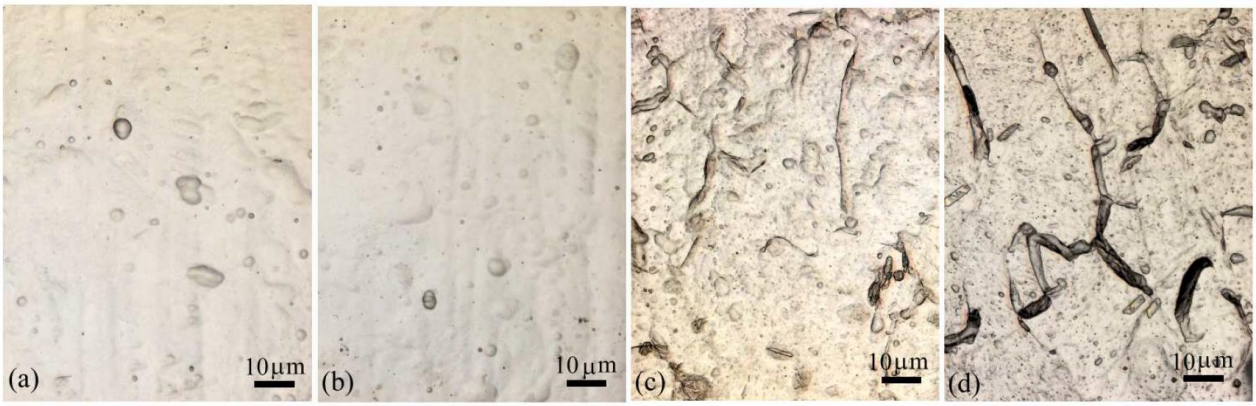

Figure 1. Surface images of the polycrystalline nickel dissolved anodically in 1.7 mol/L sulfuric acid solution at a current density of 300 mA/cm^2 and at temperatures of (a) 284 K, (b) 293 K, and (c) 306 K. (d) Surface image of polycrystalline nickel dissolved in 1.0 mol/L sulfuric acid solution at 284 K and 140 mSA/cm^2. The normalized dissolution masses were (a) 0.53, (b) 0.65, (c) 0.95, and (d) 0.17, respectively.

Grain boundary grooves in nickel anodic dissolution have been reported previously [6–9]. In our previous study, in which a rectangular pulse current was employed [17], the formation of grain boundary grooves also occurred and surfaces free of the grain boundary grooves were not observed.

Figures 1 (a) and (b) show surface images of polycrystalline nickel dissolved anodically in 1.7 mol/L sulfuric acid solution at 284 K and 293 K. No grain boundary grooves were formed and preferential dissolution at grain boundaries did not seem to occur. However, in Fig. 1 (c), grain boundary grooves were formed in polycrystalline nickel dissolved in 1.7 mol/L sulfuric acid solution at 306 K. In addition, in Fig. 1 (d), grain boundary grooves were formed in polycrystalline nickel dissolved in 1.0 mol/L sulfuric acid solution at 284 K. The normalized dissolution masses in Figs. 1 (a) and (d) were 0.53

and 0.17, respectively. This was attributed to a difference in sulfuric acid solution concentrations and showed that the grain boundary dissolution very weakly affected the total dissolution mass. The normalized dissolution masses in Figs. 1 (b) and (c) were 0.65 and 0.95, respectively. This was attributed to a difference in dissolution mechanisms such as KAP and AVP formation as stated in Section 3.2 in detail.

Grain boundaries generally have larger free energies than grain surfaces [19–20]. In the anodic dissolution of polycrystalline nickel, when a potential is applied, grain boundaries start dissolving first. In the vicinity of grain boundaries, as the dissolution rate in the direction perpendicular to the surface, $v_{\perp}$, is larger than that in the direction parallel to the surface, $v_{\parallel}$, grain boundary grooves formed after the grain boundary dissolution are observed as lines using a light microscope. There have been no studies in which grain boundary grooves are not formed in anodically dissolved polycrystalline nickel [21]. Anodic dissolution in grain boundaries has been reported to occur in sulfuric acid solution because passivation films of grain boundaries are unstable [6]. However, Figs. 1 (a) and (b) suggest that the critical temperature, Tc, and the critical sulfuric acid concentration, Cc satisfy $v_{\parallel}=v_{\perp}(Tc, Cc)$. Higher sulfuric acid concentrations and lower temperatures are needed to increase $v_{\parallel}$ and suppress $v_{\perp}$, respectively. When $v_{\parallel}$ is larger than $v_{\perp}$, grain boundary grooves are not observed using a light microscope.

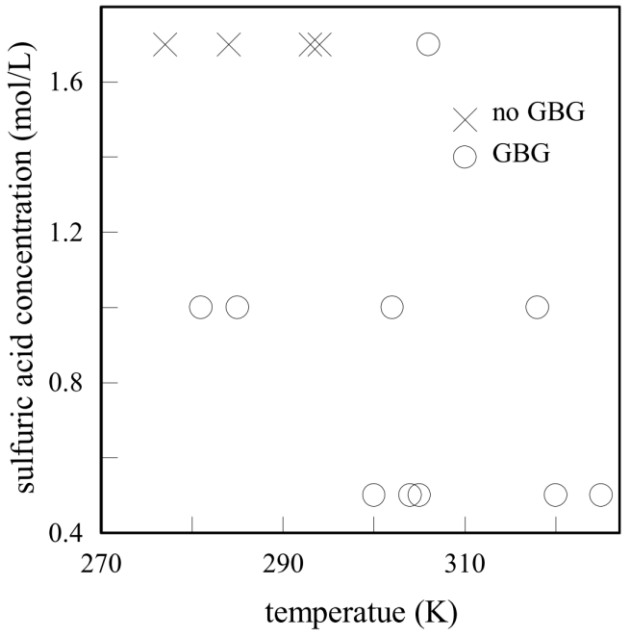

Figure 2. Phase diagram of polycrystalline nickel surfaces free of grain boundary grooves (GBG) and those with grain boundary grooves under temperatures and sulfuric acid concentrations.

Figure 2 shows a phase diagram of the grain boundary groove formed in the anodic dissolution of polycrystalline nickel under temperatures and sulfuric acid concentrations. The groove formation occurs in 0.5 mol/L and 1.0 mol/L sulfuric acid solutions irrespective of the current densities and temperatures. No grain boundary grooves were formed at temperatures ≤ 293 K and sulfuric acid solution

concentrations ≥ 1.7 mol/L. These become etching conditions to produce mirror surfaces free of grain boundary grooves.

3.2 Transition from smooth to rough surfaces in polycrystalline nickel dissolution

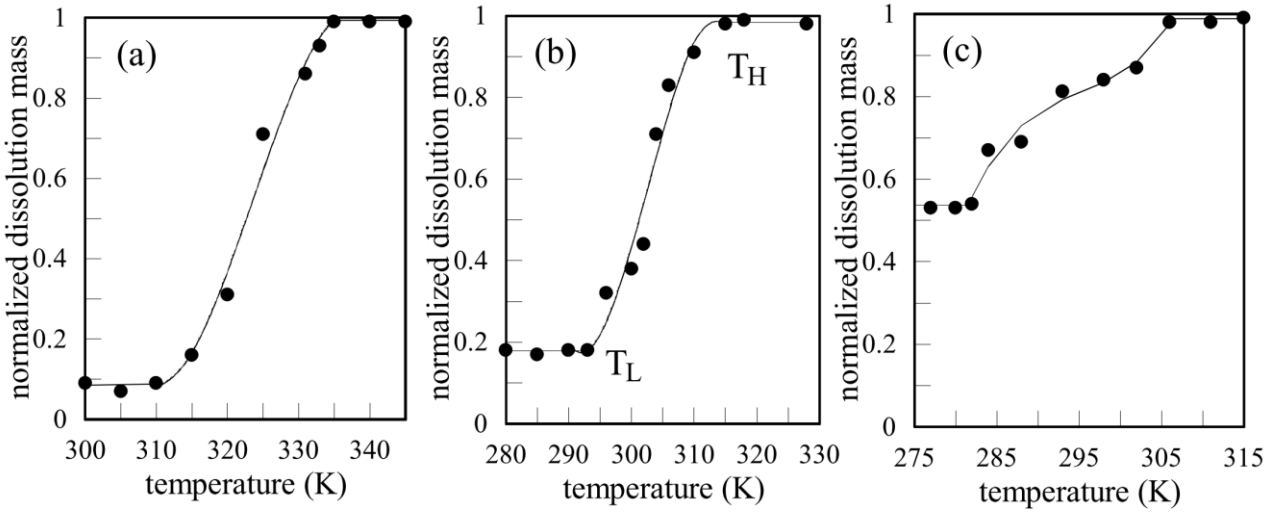

Figure 3. Temperature-dependence of the normalized dissolution mass at a current density of 140 mA/cm^2 and sulfuric acid solution concentrations of (a) 0.5 mol/L, (b) 1.0 mol/L, and (c) 1.7 mol/L. The solid lines are drawn to guide the eye. T_L and T_H denote the low and high transition temperature.

First, we briefly summarize the previous experimental results in nickel anodic dissolution [17]. Using the rectangular pulse current technique, the transition in anodic dissolution from the smooth to the rough surface emerged at a frequency over 200 Hz. Only one transition temperature from the smooth to the rough surface characterized the thermal surface roughening. However, it was unclear whether the thermal surface transition and the co-existence of the smooth and rough surfaces (i.e., two transition temperatures) occurred under a direct current (i.e., the frequency is zero).

Figure 3 shows the temperature-dependence of nickel masses dissolved at a current density of 140 mA/cm^2 in (a) 0.5, (b) 1.0, and (c) 1.7 mol/L sulfuric acid solutions. In Fig. 3 (a), the normalized dissolution masses within the temperature range of 300 – 310 K was approximately 0.08 and increased within the temperature range of 310 – 335 K. At temperatures higher than 335 K, the normalized dissolution mass was 0.99. The temperature dependence of the dissolution masses in Fig. 3 (b) and (c) was similar to that in Fig. 3 (a). The two crossover points denoted in Fig. 3 (b), T_L and T_H are defined as the low and high transition temperatures, respectively [17]. The two transition temperatures shifted to lower temperatures with an increase in sulfuric acid solution concentrations.

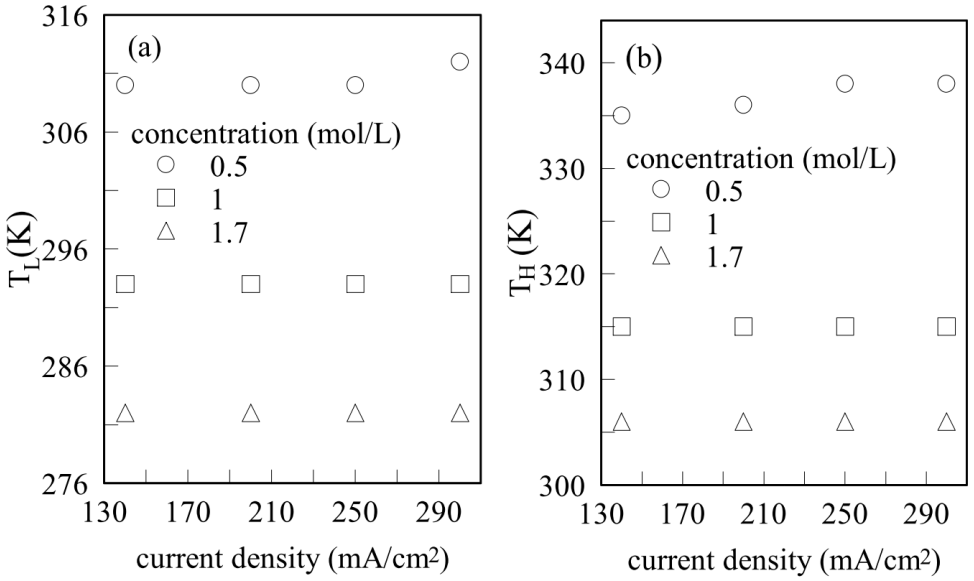

Figure 4. Plots of (a) the low and (b) high transition temperature vs. the current density for three sulfuric acid concentrations.

Figure 4 shows a plot of T_L and T_H vs. the current density in 0.5 mol/L sulfuric acid solution. Since T_L and T_H showed a very weak dependence on the current density, they had constant values within experimental errors. This shows that the current densities did not affect the binding energy between Ni atoms [22]. The normalized dissolution mass in the three regions can be combined with the two dissolution mechanisms such as the formation of KAP and AVP from the observation of the surface images as explained in the Introduction.

The surface images of polycrystalline nickel dissolved anodically at 305 K, 325 K, and 340 K in 0.5 mol/L sulfuric acid solution, and the surface heights measured along a scan line (white line) with the confocal laser scanning microscope are shown in Fig. 5. The surface images in Figs. 5 (a), (b), and (c) correspond to those in the temperature region having the lower, the intermediate, and the higher normalized dissolution mass in Fig. 3 (a), respectively.

In Fig. 5 (a), the dissolved surface comprises grains with smooth surfaces and grain boundary grooves that appeared as meandering strings. As shown in Fig. 5 (d), the groove that is as deep as a well indicates that the dissolution rate of the grain boundary is higher than that of the grain. According to the phase diagram in Fig. 2, grain boundary grooves are formed in 0.5 mol/L sulfuric acid solution at 305 K. The RMS roughness of the grain was 0.10±0.06 μm, which was much lower than that in the as-received nickel anode electrode, 0.21±0.03 μm. Hence, anodic dissolution reduced the surface roughness (i.e., caused the surface to become more smooth), except for grain boundaries.

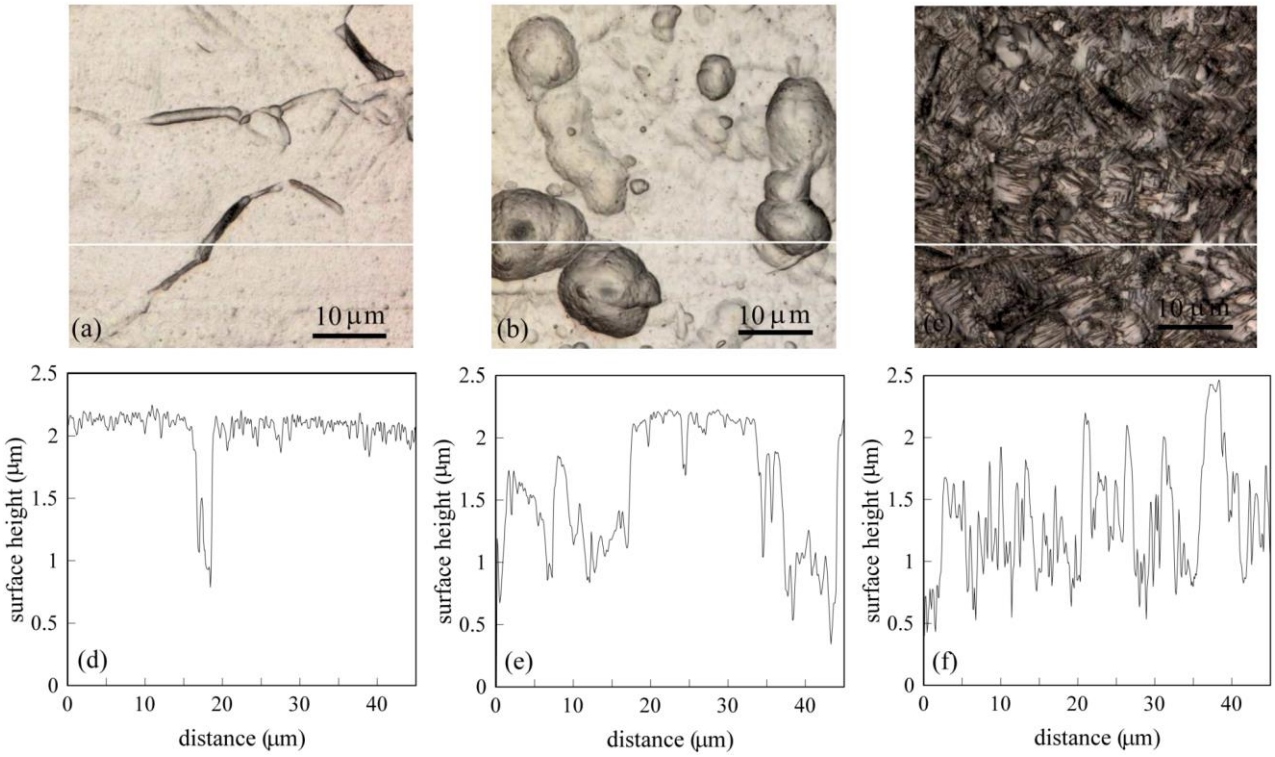

Figure 5. Surface images of the polycrystalline nickel dissolved at 140 mA/cm^2 in 0.5 mol/L sulfuric acid solution, and their surface height measured along a scan line (white line) using a CLSM. The dissolution temperatures were (a) 305 K, (b) 325 K, and (c) 340 K. Plots of the surface height vs. the distance measured along the white line in Figs. 4 (a), (b), and (c) are shown in Figs. 4 (d), (e), and (f), respectively.

A typical surface image of the grain boundary in Fig. 5 (b) and the surface profile in Fig. 5 (e) in the intermediate temperature region between T_L and T_H indicate that smooth and rough surfaces co-existed.

In contrast with Fig. 5 (a), Fig. 5 (c) shows that the surface image of the T_H at 335 K appeared prominently rough. No grain boundary and no smooth surfaces were formed as shown in Fig. 5 (f). The surface appearance had a semi-dull luster.

According to the KT transition [14], the dissolution mechanism that yields a smooth surface is thought to be due to the formation of KAP [15]. Atoms in a step edge of kink and antikink dissolve into the solution, and KAP moves step by step [13]. The motion of KAP forms the smooth terrace, and the coalescence of KAP gives rise to the smooth terrace without a step edge. At temperatures below T_L, KAP formation acted as the dissolution mechanism and resulted in a smooth surface and smaller normalized dissolution mass. On the other hand, the formation of AVP [15] that needs more bonds to be broken than KAP creation occurs at a higher temperature. As the AVP formation occurs independently at many sites on the surface, the surface roughness increases with the dissolution time. The adatom in this study is a nickel atom on the polycrystalline nickel plate and dissolves as a nickel ion into the solution. At temperatures over T_H, AVP formation is thought to act as the dissolution mechanism and results in a rough surface and larger normalized dissolution mass. In the intermediate temperature region between T_L and T_H, the two mechanisms co-exist as shown in the surface profile in Fig. 5 (e).

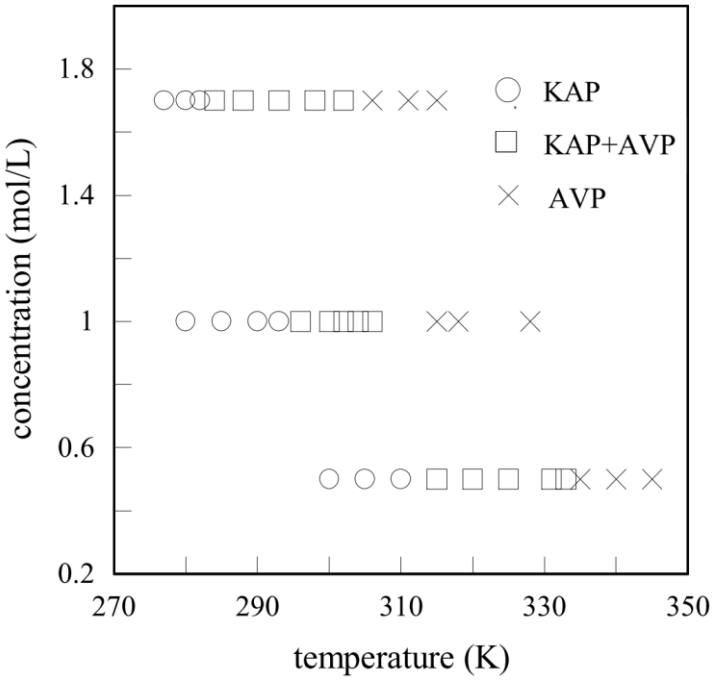

Figure 6. Phase diagram of dissolution modes of polycrystalline nickel under temperatures and sulfuric acid concentrations.

Figure 6 shows dominant dissolution modes under the temperatures and sulfuric acid concentrations. The transition from KAP to AVP is attributed to an increase in the temperature. This is because the formation of AVP needs larger energy than that of KAP [15–16, 22]. With an increase in the sulfuric acid concentration, the stable states of KAP and AVP become narrow and wide, respectively. As shown in Fig. 6, fast dissolution of polycrystalline nickel can be done in the stable state of AVP.

4. CONCLUSIONS

Two phase-diagrams of the thermal surface roughening transition in polycrystalline nickel anodic dissolution in sulfuric acid solution were made using DMM and a CLSM. No grain boundary groove was found at the temperatures ≤ 293 K and sulfuric acid solution concentrations ≥ 1.7 mol/L. The change in the normalized dissolution mass at the transition temperatures corresponded to that in the surface roughness. These changes are thought to be caused by the formation of KAP and AVP. In the intermediate region between T_L and T_H, the two formation mechanisms co-existed.

ACKNOWLEDGMENTS
The author thanks Miss N. Yatsuka for the experimental setup.

References

1. C. Gu and J. Tu, *Langmuir*, 27 (2011) 10132.
2. Z. Jahed, R. Lin, B. B. Seo, M. S. Verma, F. X. Gu, T. Y. Tsui, and M. R. K. Mofrad, *Biomater.*, 35 (2014) 4240.
3. V. Gowthami, M. Meenakshi, P. Perumal, R. Sivakuma, and C. Sanjeeviraja, *Mater. Sci. Semicond. Proc.*, 27 (2014) 1042.
4. K. Juodkazis, L. Juodkazyté, R. Vilkauskaité, and V. Jasulaitiené, *J. Solid. Stat. Electrochem.*, 12 (2008) 1469.
5. M-S. Wu, Y-A. Huang, C-H. Yang, and J-J Jow, *Int. J. Hydrog. Energy*, 32 (2007) 4153.
6. P. Marcus and V. Maurice, *Phil. Trans. R. Soc. A*, **375**: 20160414.
7. A. K. Pramanick, A. Sinha, G. V. S. Sastry, and R. N. Ghosh, *Ultramicroscopy*, 109 (2009) 741.
8. T. A. Roth, *Mater. Sci. Eng.*, 18 (1975) 183.
9. D. Amram, L. Klinger, N. Gazit, H. Gluska, and E. Rabkin, *Acta. Mater.*, 69 (2014) 386.
10. D. Bilczuk, O. G. Olvera, and E. Asselin, *Can. J. Chem. Eng.*, 94 (2016) 1872.
11. M. Saitou, A. Makabe, and T. Tomoyose, *J. Chem. Phys.*, 113 (2000) 2397.
12. K. Hedayati and G. Nabiyouni, *Appl. Phys. A*, 116 (2014) 1605.
13. W. K. Burton, N. Cabrera, and F. C, Frank, *Phil. Trans. Roy. Soc. (London) A*, 243 (1951) 299.
14. J. M. Kosterlitz and D. J. Thouless, *J. Phys. C*, 6 (1973) 1181.
15. D. L. Blanchard, D. F. Thomas, and H. Xu, T. Engel, *Surf. Sci.*, 222 (1989) 470.
16. E. H. Conrad, L. R. Allen, D. L. Blanchard, and T. Engel, *Surf. Sci.*, 187 (1987) 265.
17. M. Saitou, *J. Phys. D*, 44 (2011) 455302.
18. A. G. Muñoz, G. Benitez, M. E. Vela, and R. C. Salvarezza, *Langmuir*, 20 (2004) 2361.
19. V. V. Bulatov, B. W. Reed, and M. Kumar, *Acta Mater.*, 65 (2014) 161.
20. E. A. Holm, D. L. Olmsted, and S. M. Foiles, *Scr. Mater.*, 63 (2010) 905.
21. Q. Li-yuan, L. Jian-she, and J. Qing, *Trans. Nonferrous Met. Soc. China*, 20 (2010) 82.
22. L. Beaunier, *J. Phys. Colloq.*, 43 (1982) 271